

RESEARCH

Open Access



# Global metabolic alterations in colorectal cancer cells during irinotecan-induced DNA replication stress

Christian Marx<sup>1,2,3,4\*</sup> , Jürgen Sonnemann<sup>5,6</sup>, Oliver D. K. Maddocks<sup>7</sup>, Lisa Marx-Blümel<sup>5,6</sup>, Mandy Beyer<sup>1</sup>, Doerte Hoelzer<sup>8,9</sup>, René Thierbach<sup>8</sup>, Claudia Maletzki<sup>10,11</sup>, Michael Linnebacher<sup>10</sup>, Thorsten Heinzel<sup>2</sup> and Oliver H. Krämer<sup>1,2\*</sup> 

## Abstract

**Background:** Metabolic adaptations can allow cancer cells to survive DNA-damaging chemotherapy. This unmet clinical challenge is a potential vulnerability of cancer. Accordingly, there is an intense search for mechanisms that modulate cell metabolism during anti-tumor therapy. We set out to define how colorectal cancer CRC cells alter their metabolism upon DNA replication stress and whether this provides opportunities to eliminate such cells more efficiently.

**Methods:** We incubated p53-positive and p53-negative permanent CRC cells and short-term cultured primary CRC cells with the topoisomerase-1 inhibitor irinotecan and other drugs that cause DNA replication stress and consequently DNA damage. We analyzed pro-apoptotic mitochondrial membrane depolarization and cell death with flow cytometry. We evaluated cellular metabolism with immunoblotting of electron transport chain (ETC) complex subunits, analysis of mitochondrial mRNA expression by qPCR, MTT assay, measurements of oxygen consumption and reactive oxygen species (ROS), and metabolic flux analysis with the Seahorse platform. Global metabolic alterations were assessed using targeted mass spectrometric analysis of extra- and intracellular metabolites.

**Results:** Chemotherapeutics that cause DNA replication stress induce metabolic changes in p53-positive and p53-negative CRC cells. Irinotecan enhances glycolysis, oxygen consumption, mitochondrial ETC activation, and ROS production in CRC cells. This is connected to increased levels of electron transport chain complexes involving mitochondrial translation. Mass spectrometric analysis reveals global metabolic adaptations of CRC cells to irinotecan, including the glycolysis, tricarboxylic acid cycle, and pentose phosphate pathways. P53-proficient CRC cells, however, have a more active metabolism upon DNA replication stress than their p53-deficient counterparts. This metabolic switch is a vulnerability of p53-positive cells to irinotecan-induced apoptosis under glucose-restricted conditions.

**Conclusion:** Drugs that cause DNA replication stress increase the metabolism of CRC cells. Glucose restriction might improve the effectiveness of classical chemotherapy against p53-positive CRC cells.

**Keywords:** Adaptation, Colorectal cancer, Glucose, Irinotecan, Metabolism, p53, Warburg effect

\*Correspondence: christian.marx@zepai.de; okraemer@uni-mainz.de

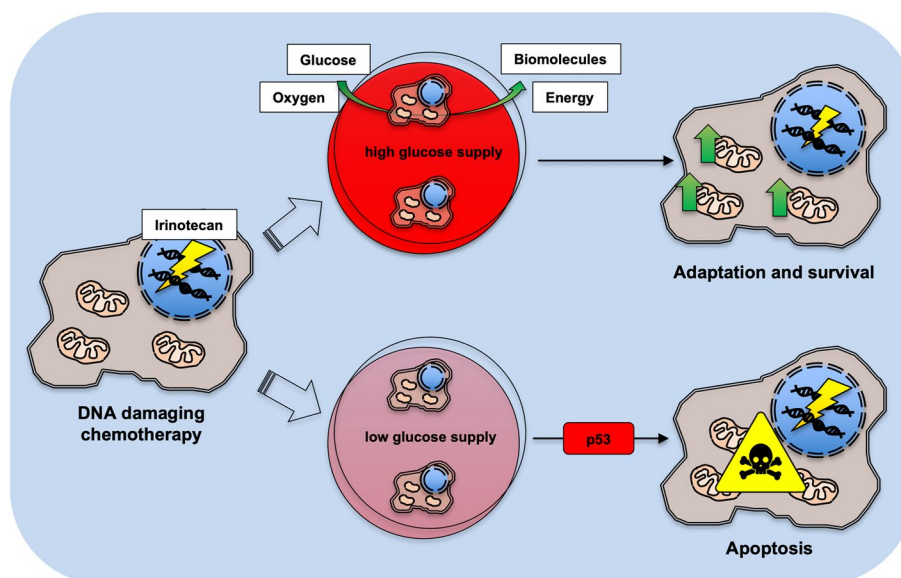
<sup>1</sup> Department of Toxicology, University Medical Center, Johannes Gutenberg University Mainz, Building 905, Mainz, Germany  
Full list of author information is available at the end of the article



© The Author(s) 2022. **Open Access** This article is licensed under a Creative Commons Attribution 4.0 International License, which permits use, sharing, adaptation, distribution and reproduction in any medium or format, as long as you give appropriate credit to the original author(s) and the source, provide a link to the Creative Commons licence, and indicate if changes were made. The images or other third party material in this article are included in the article's Creative Commons licence, unless indicated otherwise in a credit line to the material. If material is not included in the article's Creative Commons licence and your intended use is not permitted by statutory regulation or exceeds the permitted use, you will need to obtain permission directly from the copyright holder. To view a copy of this licence, visit <http://creativecommons.org/licenses/by/4.0/>. The Creative Commons Public Domain Dedication waiver (<http://creativecommons.org/publicdomain/zero/1.0/>) applies to the data made available in this article, unless otherwise stated in a credit line to the data.

## Graphical Abstract

The topoisomerase-1 inhibitor irinotecan and other chemotherapeutics that cause DNA damage induce metabolic adaptations in colorectal cancer (CRC) cells irrespective of their p53 status. Irinotecan enhances the glycolysis and oxygen consumption in CRC cells to deliver energy and biomolecules necessary for DNA repair and their survival. Compared to p53-deficient cells, p53-proficient CRC cells have a more active metabolism and use their intracellular metabolites more extensively. This metabolic switch creates a vulnerability to chemotherapy under glucose-restricted conditions for p53-positive cells.



## Introduction

Metabolism serves to fuel cells with energy and the building blocks for biosynthesis. The fine-tuned balance between catabolic and anabolic processes involves several interconnected pathways, with mitochondria as cellular powerhouses for efficient energy retrieval. Glucose, a main source of cellular energy, is degraded via glycolysis or metabolized within the pentose phosphate pathway (PPP) [1, 2]. Glycolysis produces two molecules of pyruvate and of the energy-rich molecules ATP and NADH. This process consumes two molecules ADP and  $\text{NAD}^+$  per molecule glucose. To quickly regenerate  $\text{NAD}^+$ , cells can metabolize pyruvate to lactate [1]. The more efficient, but slower oxidative turnover of pyruvate fuels the tricarboxylic acid (TCA) cycle and the oxidative phosphorylation (OXPHOS) within the mitochondrial electron transport chain (ETC). This pathway yields about 32 molecules of ATP per molecule glucose [1, 3]. ETC enzymes, like complex IV, are regulated allosterically to adjust the cell metabolism to the cellular energy level and to the availability of metabolites [4].

Despite a higher ATP yield from mitochondrial respiration over glycolysis, cancer cells tend to perform glycolysis even in the presence of sufficient oxygen. In the

1920s, Otto Warburg first described this hallmark of cancer, which is called aerobic glycolysis or the Warburg effect [1, 5–7]. This glycolytic metabolism delivers ATP and molecules for biosynthesis faster without reactive oxygen species (ROS) production, which can cause lethal DNA damage in fast dividing cancer cells that frequently have mutations in DNA repair proteins [6, 8–10]. In addition, this dysregulated cell metabolism supports fast cancer cell proliferation, even under hypoxic conditions in solid tumor masses [1, 10–12]. Nevertheless, cancer cells retain a certain capacity to activate their OXPHOS after stress, e.g., for DNA repair, and cancer cell metabolism is more complex and flexible than initially believed [1, 6, 7, 10, 13–17]. Hence, metabolic adaptations can help cancer cells to escape DNA-damaging drugs [3, 10, 18–22]. Damages to the ETC and mitochondrial DNA (mtDNA) can in turn increase the chemosensitivity of tumor cells [3, 10]. Accordingly, there is an intense search for mechanisms and metabolic inhibitors for anti-tumor therapy [16, 23].

Colorectal cancer (CRC) is the second most common cause of cancer death. Alone in the USA, approximately 147,950 individuals were diagnosed with CRC and 53,200 died from the disease in 2020 [24]. Defining

and exploiting metabolic adaptation might save millions of lives each year. It is reported that caloric restriction (CR) and fasting periods increase the effectiveness of chemotherapy, by protecting non-malignant cells and by increasing autophagy and apoptosis in tumor cells [25–27]. However, it is still a matter of debate whether CR or fasting in combination with chemotherapy may have a beneficial or an unfavorable outcome [28].

The tumor suppressor protein p53 is a master regulator of cell metabolism, mitochondrial integrity, and antioxidant responses to ROS. Moreover, p53 regulates key metabolic pathways including the OXPHOS, glycolysis, PPP, TCA cycle, and glutaminolysis under physiologic conditions and during stress [8–10, 29–31]. Whether p53 affects metabolic adaptation of CRC cells upon chemotherapy with drugs that cause DNA replication stress is unclear.

We set out to investigate metabolic alterations after drug-induced DNA replication stress, and the role of p53 in these processes. We analyzed the responses of human p53 wild-type (HCT116<sup>wt</sup>) and otherwise isogenic p53 null (HCT116<sup>Δp53</sup>) HCT116 CRC cells to clinically approved DNA-damaging chemotherapeutics. These include the topoisomerase-1 (TOP1) inhibitor irinotecan, the ribonucleotide reductase (RNR) inhibitor hydroxyurea, and the topoisomerase-2 (TOP2) inhibitor doxorubicin [32–35]. Independent of p53, CRC cells increased their metabolic activities when exposed to these agents. Compared to p53-negative cells, p53-proficient cells were more reliant on extracellular glucose level for their survival upon DNA replication stress.

## Results

### Irinotecan treatment leads to increased mitochondrial activity

Metabolic processes can determine the fate of tumor cells with DNA replication stress, but it is ill defined how irinotecan modulates such adaptations. Therefore, we asked if irinotecan alters mitochondrial functions and used HCT116<sup>wt</sup> and HCT116<sup>Δp53</sup> CRC cells as test-bed. A direct way to measure the metabolism and ETC activity is to analyze mitochondrial oxygen consumption in cells. We found that irinotecan significantly increased this parameter after 24-h treatment in both HCT116 cell lines; HCT116<sup>wt</sup> cells showed a trend to higher respiration than HCT116<sup>Δp53</sup> cells (Fig. 1A). This was not due to differences in the accumulation of DNA replication stress/DNA damage, as evidenced by a similar accumulation of γH2AX in irinotecan-treated CRC cells with or without p53 (Fig. S1A). Moreover, oxygen consumption did not increase during the first 4 h after the application

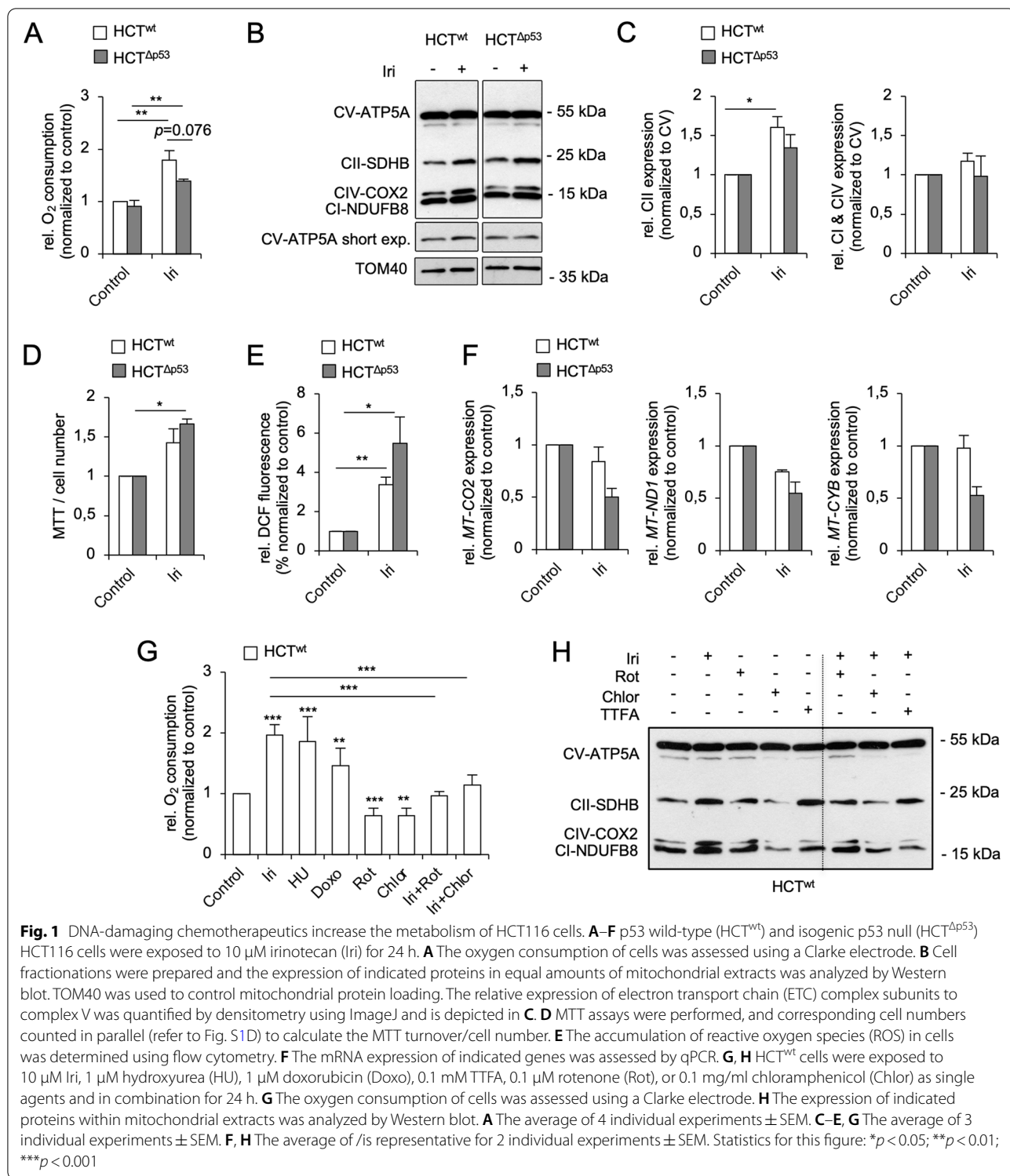
of irinotecan (Fig. S1B), indicating an adaptive process over time.

Oxygen is consumed in the ETC complex IV and requires an electron flow through the first four ETC complexes [1, 3, 36, 37]. To study whether irinotecan altered the protein levels of ETC complex subunits, we analyzed mitochondrial extracts by immunoblotting and compared ETC protein expressions to the mitochondrial outer membrane protein TOM40 (Fig. 1B, C). While ETC complex V (CV; ATP synthase subunit ATP5A) expression was not affected by irinotecan, the expression levels of complex I (CI; NADH dehydrogenase (NDH) subunit NDUFB8), II (CII; succinate dehydrogenase (SDH) subunit SDHB), and IV (CIV; cytochrome *c* oxidase (COX) subunit 2) subunits were increased relative to complex V in both HCT116 cell lines upon treatment with irinotecan. ETC CII, which is part of both the TCA cycle and the OXPHOS machinery [1, 3, 36, 37], showed the strongest increase after irinotecan treatment (Fig. 1B, C). As seen for oxygen consumption rates (Fig. 1A), HCT116<sup>wt</sup> cells showed a higher increase in ETC protein expression than p53-deficient cells in response to irinotecan.

To see whether this induction of ETC complexes also occurs in vivo, we transplanted short-term cultured human CRC cells (HROC24 (p53 wild-type) and HROC87 (p53 mutated) [38]) in mice, treated them with irinotecan, excised the tumors, and probed for ETC proteins by immunoblot. Like in cultured cells, irinotecan augmented the expression of ETC proteins in xenografted CRC cells (Fig. S1C).

Figure 1B illustrates that irinotecan particularly induces the expression of ETC CII in HCT116 cells. For a functional analysis, we studied the regulation of the ETC CII by irinotecan with the MTT assay, which also gives information about the intracellular redox balance [39]. In parallel, cell numbers were counted to subtract proliferation-dependent effects. We observed an increased MTT/cell number turnover, which was higher in HCT116<sup>Δp53</sup> cells (Figs. 1D and S1D). Since HCT116<sup>wt</sup> cells showed higher ETC protein expressions and OXPHOS activities than p53-deficient cells (Fig. 1A), we tested if the high MTT/cell number turnover originated from changes of the intracellular redox balance. The measurement of cytosolic ROS level by flow cytometry indeed showed that irinotecan induced a significant ROS increase in both CRC cell lines, with HCT116<sup>Δp53</sup> cells being more affected (Fig. 1E).

These data indicate that irinotecan induces an increase in ETC activity in CRC, which is accompanied by an accumulation of ROS, and that p53 fine-tunes these effects.



### Irinotecan treatment impairs mitochondrial gene transcription

Mitochondria are the primary source and a target of ROS-induced damages [40, 41]. If the increased ETC

protein levels after irinotecan treatment (Fig. 1B, C) are due to an increased transcription of mtDNA-encoded genes or an increase in mitochondria *per se*, there should be an increased number of mitochondrial mRNAs after

irinotecan treatment. The human mtDNA harbors 39 genes, of which 13 code for the essential core subunits of the ETC complexes: I (*MT-ND1*, *MT-ND2*, *MT-ND3*, *MT-ND4*, *MT-ND4L*, *MT-ND5*, and *MT-ND6*), III (*MT-CYB*), IV (*MT-COI*, *MT-COII*, and *MT-COIII*), and V (*MT-ATP6* and *MT-ATP8*) (MITOMAP: a human mitochondrial genome database; <http://www.mitomap.org>). The assembly of ETC complexes is a highly complicated and well-coordinated process. Changes in the expression of the mtDNA-encoded subunits affect the assembly of the whole ETC super-complexes [36, 37].

Analyses with quantitative polymerase chain reaction (qPCR) showed that irinotecan decreased the mitochondrial encoded *MT-COII* (*COX2*), *MT-ND1* (*NDH* subunit 1), and *MT-CYB* (cytochrome *b*) mRNA levels in HCT116<sup>Δp53</sup> cells (Fig. 1F). HCT116<sup>wt</sup> cells had moderately decreased *MT-COII* and *MT-ND1* expression levels after irinotecan treatment, disfavoring that irinotecan enhanced the mtDNA gene expression.

This decrease of mtDNA transcripts (Fig. 1F) made us hypothesize that increased translation contributed to the higher levels of ETC proteins and increased respiration. We used chloramphenicol, which inhibits mitochondrial ribosomes [42], to analyze whether irinotecan increases the mitochondrial protein translation (Figs. 1G, H, and S1E). Congruent with our hypothesis, chloramphenicol reduced the oxygen consumption in both irinotecan-treated HCT116 cell lines significantly, and chloramphenicol alone as well as in combination with irinotecan suppressed the expression of ETC CI-IV. The expression of ETC CV was again unaffected by any treatment (Fig. 1H), indicating a longer protein half-life compared with the other tested ETC complex subunits. In addition, the use of the ETC CI inhibitor rotenone and the ETC CII inhibitor 2-thenoyltrifluoroacetone (TTFA) [43] showed that the activity of both ETC complexes significantly contributed to the DNA damage-induced increase in oxygen consumption (Figs. 1G and S1E-F). Noteworthy, neither rotenone nor TTFA suppressed the induction of ETC CI-IV proteins by irinotecan (Fig. 1H).

We also measured the mitochondrial respiration after exposure to hydroxyurea and doxorubicin, which cause DNA replication stress and DNA damage [33, 34]. Both agents increased the oxygen consumption significantly

and p53-independently (Figs. 1G and S1E), indicating a general increase of respiration after DNA replication stress/DNA damage.

These data illustrate that enhanced ETC protein expression in response to irinotecan is connected to the translation of mtDNA.

#### Irinotecan increases both glycolysis and respiration in HCT116 cells

We speculated that irinotecan might induce global metabolic adaptations. To test this, we analyzed the metabolic flux of HCT116 cells in real time with a Seahorse Analyzer. This system allows parallel measuring of oxygen consumption (OCR) and extracellular acidification rates (ECAR). The latter results from fermentative glycolysis and lactate secretion [44, 45].

To study mitochondrial parameters, we performed a Cell Mito Stress Test (Figs. 2A–C and S2A–B). We found that HCT116<sup>wt</sup> cells had higher basal OCR and ECAR than p53-deficient cells (Figs. 2A, B, and S2B). Irinotecan increased these values in both CRC cell lines significantly (Figs. 2A, B, and S2B). The ATP production in HCT116<sup>wt</sup> cells was higher than in cells without p53, and irinotecan increased this parameter significantly in both CRC cell lines (Fig. 2C). Unexpectedly, the respiratory spare capacity was negative in both HCT116 cell lines and lower in p53 wild-type cells (Fig. 2A, C). This suggests that HCT116 cells preferentially use glycolysis and cannot sustain their mitochondrial integrity upon DNA replication stress. Further details on this aspect are provided below.

Irinotecan also increased the metabolism of p53 wild-type RKO CRC cells (Fig. S2C–D). Unlike HCT116 cells, these cells mainly increased their OXPHOS activity in response to the DNA replication stress, which was accompanied by an increased ATP production and respiratory spare capacity (Fig. S2E).

To study glycolytic functions in more detail, we performed a Glycolysis Stress Test (Figs. 2D–F and S2F–G). We found that during the first period of this assay, when L-glutamine was the only available energy resource, both irinotecan-treated and control HCT116<sup>wt</sup> cells had a significantly higher OCR (glutamine-driven respiration) than HCT116<sup>Δp53</sup> cells (Figs. 2D–F and S2F–G). After the

(See figure on next page.)

**Fig. 2** Irinotecan activates both respiration and glycolysis in HCT116 cells. p53 wild-type (HCT<sup>wt</sup>) and isogenic p53 null (HCT<sup>Δp53</sup>) HCT116 cells were exposed to 10 μM irinotecan (Iri) for 24 h. **A** Oxygen consumption (OCR) and **B** extracellular acidification rates (ECAR) were assessed with a Cell Mito Stress Test using a Seahorse XFe24 Analyzer. 2 μM oligomycin, 2 μM FCCP, and 2 μM antimycin A were injected consecutively during the measurement. **C** Bioenergetic parameters, i.e., ATP production and respiratory spare capacity, were calculated from OCR/ECAR curves shown in **A** and **B**. **D** OCR and **E** ECAR were assessed with a Glycolysis Stress Test using a Seahorse XFe24 Analyzer. 10 mM D-glucose, 2 μM oligomycin, and 50 mM 2-DG were injected consecutively during the measurement. **F** Bioenergetic parameters, i.e., glycolysis, respiration difference (before and after glucose injection) and glycolytic reserve, were calculated from OCR/ECAR curves shown in **D** and **E**. All figures show the average of 3 individual experiments ± SEM. Statistics for this figure: \**p* < 0.05; \*\**p* < 0.01; \*\*\**p* < 0.001

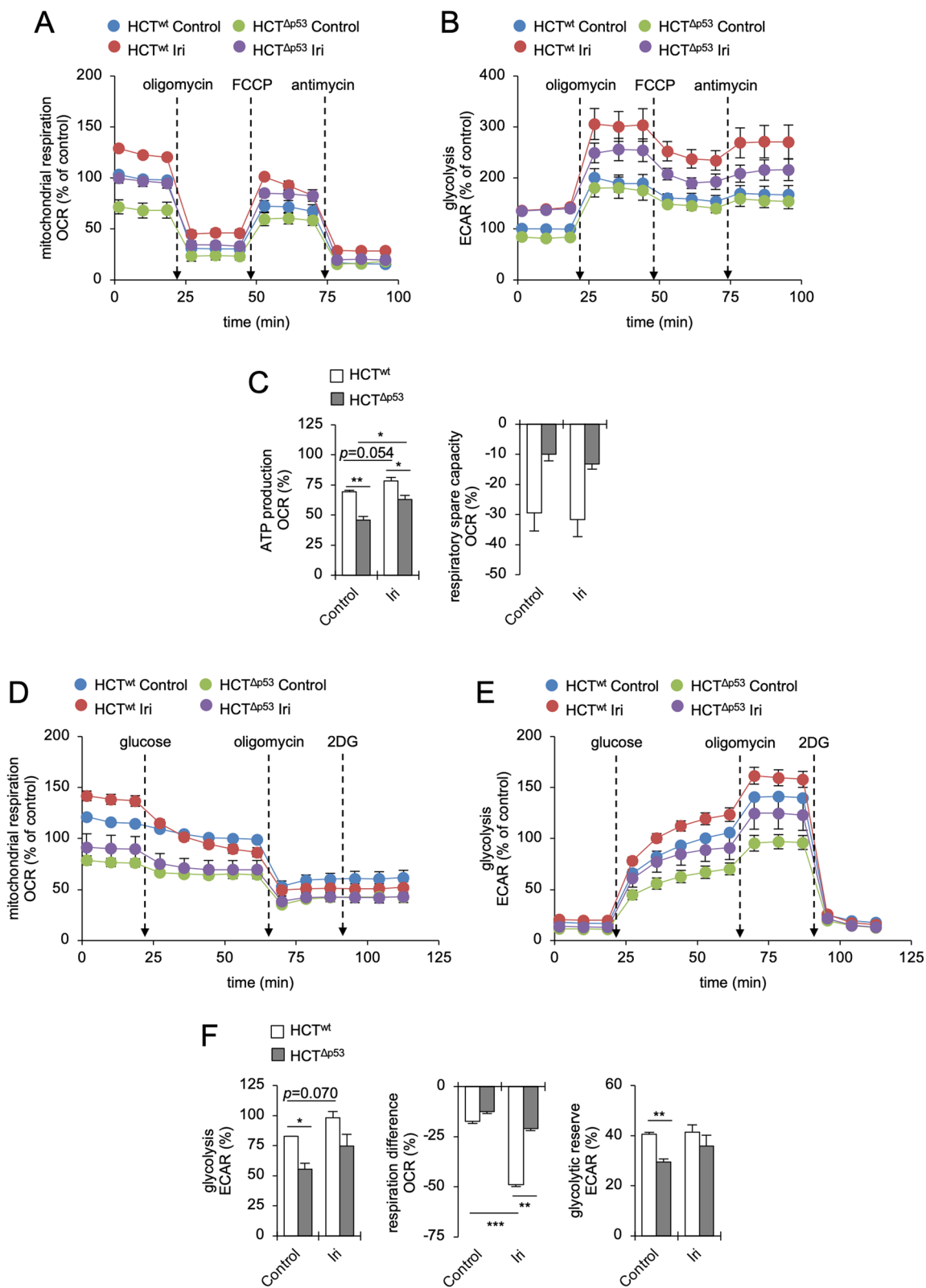


**Fig. 2** (See legend on previous page.)

addition of glucose, HCT116<sup>wt</sup> cells maintained a higher OCR (glucose-driven respiration) and ECAR (glycolysis) than p53-deficient cells (Figs. 2D–F and S2F–G). Although irinotecan enhanced ECAR values in both HCT116 cell lines, we observed a significant decrease of OCR specifically in irinotecan-treated HCT116<sup>wt</sup> cells (50.2% OCR decrease) after the addition of glucose (Figs. 2D, F, and S2G). HCT116<sup>Δp53</sup> cells did not show this response to glucose (Fig. 2D). The glycolytic reserve, which indicates the capacity of cells to compensate OXPHOS defects by glycolysis, was significantly higher in untreated p53-proficient cells than in HCT116<sup>Δp53</sup> cells (Fig. 2F).

Finally, to separate and analyze mitochondrial functions of HCT116 cells under conditions supporting either a glycolysis- or an OXPHOS-driven metabolism, we customized a Cell Mito Stress Test. On the one hand, cells were supplied with glucose (no pyruvate in the medium) feeding the (aerobic) glycolysis and the TCA cycle. On the other hand, cells were supplied with pyruvate (no glucose in the medium) selectively feeding the TCA cycle and subsequently the OXPHOS. Both conditions were analyzed side-by-side in control and irinotecan-treated HCT116 cells (Fig. S3). In the first setting, when glucose was the main energy source (Fig. S3A–E), we made similar observations as seen before (compare with Figs. 2A–C and S2A–B): p53-proficient cells had a more active metabolism than p53-deficient cells, both had negative respiratory spare capacities, and the treatment with irinotecan increased the OCR of HCT116 cells (Fig. S3B–E). Intriguingly, we found in the second setting (Fig. S3F–J) that HCT116 cells had a significantly higher OCR than before (about 100% increase), which was further increased especially in irinotecan-treated HCT116<sup>wt</sup> cells. In addition, the mitochondrial ATP production was greatly increased, and cells shifted into prominent and positive respiratory spare capacities (compare Figs. 2A–C, S3B, and E with G and J). The treatment with irinotecan increased the ATP production and respiratory spare capacities particularly in p53-proficient HCT116 cells. As expected, ECAR values were dramatically decreased in the absence of glucose confirming that only small amounts of pyruvate were converted into lactate and mainly used to feed the TCA cycle and OXPHOS (Fig. S3H).

These data show that despite high levels of respiration, p53-positive CRC cells switch to glycolysis in the presence of glucose. During DNA replication stress, HCT116<sup>wt</sup> cells prefer to consume glucose aerobically and are less reliant on their mitochondria. If glucose is not available, these cells strongly increase their respiration.

#### Mass spectrometry reveals global metabolic adaptations to DNA replication stress/DNA damage

To study the cell metabolism of irinotecan-treated HCT116 cells in a global manner, we performed a targeted mass spectrometric analysis of selected metabolites (metabolomics). After 24 h, we analyzed changes of metabolites in the cell culture medium (Fig. 3A, B) as well as in irinotecan-treated HCT116 cells (Fig. 3C). The results of our analysis are summarized in Fig. 4A.

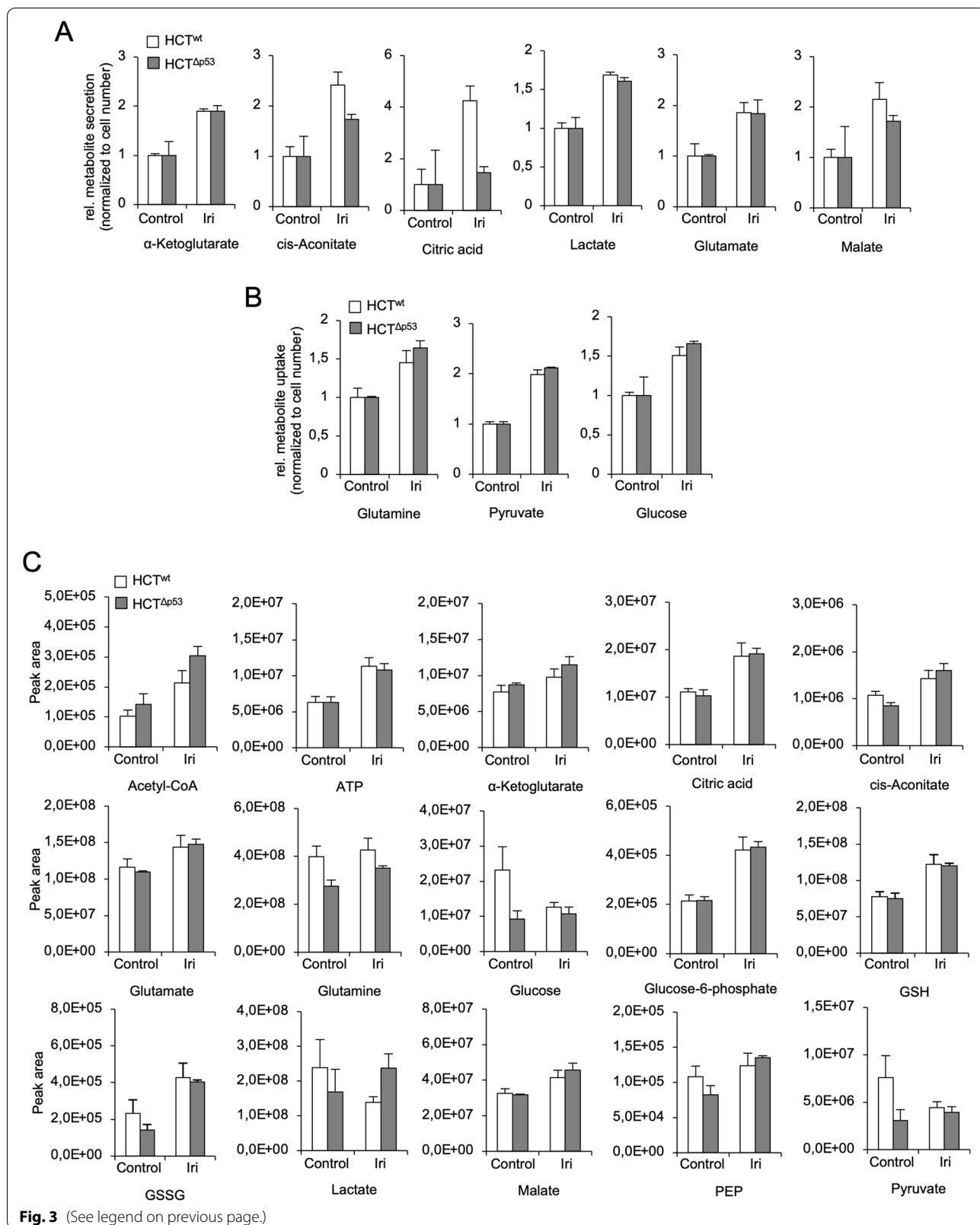
Both CRC cell lines consumed higher levels of glutamine, pyruvate, and glucose and secreted more  $\alpha$ -ketoglutarate, cis-aconitate, citric acid, lactate, glutamate, and malate from/into the culture medium after irinotecan application. HCT116<sup>wt</sup> cells secreted more cis-aconitate, citric acid, and malate than HCT116<sup>Δp53</sup> cells (Fig. 3A, B). Among intracellular metabolites, we observed that acetyl-CoA,  $\alpha$ -ketoglutarate, cis-aconitate, citric acid, glutamine/glutamate, glucose-6-phosphate, malate, and phosphoenolpyruvate (PEP) increased in both HCT116 cell lines similarly after irinotecan treatment together with intracellular ATP level (Fig. 3C). This data is congruent to our Seahorse analysis (Fig. 2). High amounts of glucose-6-phosphate together with an increased level of reduced and oxidized glutathione (GSH/GSSG) show that irinotecan also activated the PPP (Fig. 3C).

Intriguingly, we found that untreated HCT116<sup>wt</sup> cells had a higher level of intracellular glucose, pyruvate, and lactate than p53-deficient cells. All these metabolites decreased in HCT116<sup>wt</sup> cells after irinotecan treatment (Fig. 3C). In contrast to this, glucose and pyruvate levels in HCT116<sup>Δp53</sup> cells were stable after irinotecan application, whereas lactate level moderately increased.

These results illustrate that the irinotecan-induced DNA replication stress globally activates several

(See figure on next page.)

**Fig. 3** Mass spectrometry confirms increased cell metabolism after irinotecan treatment. **A–C** p53 wild-type (HCT<sup>wt</sup>) and isogenic p53 null (HCT<sup>Δp53</sup>) HCT116 cells were exposed to 10  $\mu$ M irinotecan (Iri). The abundance of indicated metabolites in the supernatant cell culture medium (**A**, **B**) and in cells (**C**) was assessed after 24 h by targeted mass spectrometric analysis (metabolomics). Alterations of metabolite secretion and uptake after treatment are depicted in **A** and **B**, respectively. Metabolites present in the DMEM medium (high glucose) at the beginning of the experiment were subtracted from the data shown in **A** and **B**. Changes of intracellular metabolites are shown in **C**. Abbreviations: GSH/GSSG reduced/oxidized glutathione, PEP phosphoenolpyruvate. **A–C** The average of 3 individual experiments  $\pm$  SEM



metabolic pathways and that p53-proficient CRC cells use their metabolites in a more extensive manner.

#### HCT116<sup>wt</sup> cells rely on glucose for their survival after DNA damage

The data above show that p53-proficient HCT116 cells have a significantly higher (glycolytic) metabolism after DNA replication stress/DNA damage than HCT116<sup>Δp53</sup> cells (Figs. 1, 2, 3, and 4A). Thus, we investigated if HCT116<sup>wt</sup> cells could be sensitized to irinotecan by lowering glucose availability. We cultivated both HCT116 cell lines in medium with high (4.5 g/l) or low (1 g/l) glucose and treated them for up to 48 h with irinotecan (Fig. 4B–E). We measured mitochondrial depolarization (loss of  $\Delta\Psi_M$ ) as an early apoptosis marker and PI uptake for total cell death by flow cytometry. After 24-h treatment with irinotecan in a low-glucose medium, HCT116<sup>wt</sup> cells showed significantly higher levels of  $\Delta\Psi_M$  loss than cells that were cultivated in high glucose (Fig. 4B). The oxygen consumption of these cells was slightly increased when cultured in a medium with low glucose (Fig. 4C). Compared to cells cultivated in high glucose, irinotecan-treated HCT116<sup>wt</sup> cells in a medium with low glucose had significantly higher levels of  $\Delta\Psi_M$  loss and cell death after 48 h (Fig. 4D). In addition, we observed that untreated HCT116<sup>wt</sup> cells in the low-glucose medium had significantly more  $\Delta\Psi_M$  loss and cell death than cells that were cultured in the high-glucose medium. This correlates with a decreased oxygen consumption of HCT116<sup>wt</sup> cells after 48 h of culture in a medium with low glucose levels (Fig. 4E) suggesting that the remaining glucose level in the culture medium of p53-positive cells after 48 h was insufficient to fuel their mitochondrial metabolism properly and might become a limiting factor for these cells. HCT116<sup>Δp53</sup> cells did not show any significant increase in cell death or  $\Delta\Psi_M$  loss after 24–48-h irinotecan treatment, irrespective of glucose levels in the culture media (Fig. 4B, D). These data show that p53-proficient CRC cells need glucose to remain viable during DNA replication stress/DNA damage.

#### Discussion

Irinotecan is frequently applied to treat CRC. Unfortunately, it produces severe side effects that compromise its use [32, 35, 46]. Fasting can reduce the severity of such side effects without affecting its anti-tumor efficiency in xenograft mouse models [47]. Moreover, CR and fasting were shown to increase the anti-tumor effectiveness of chemotherapy [25–27]. Thus, the tumor metabolism is an appealing target in combination with classical chemotherapeutic agents to improve the treatment outcome in patients [14–16, 20, 26, 28, 48].

The common view on cancer cell metabolism is that malignant cells increase their glycolysis and decrease their respiration during transformation to reduce intracellular ROS level and to proliferate quickly, which is one hallmark of cancer [1, 5, 6, 11, 13]. Nevertheless, cancer cell metabolism is more complex and flexible [1–3, 6, 10, 13, 16–18, 30, 49]. In this context, we asked how irinotecan changes mitochondrial functions of CRC cells and how we could modulate its effectiveness via manipulating their metabolism. We show that the clinically approved drugs [32–34], irinotecan, hydroxyurea, and doxorubicin, increase the respiration of CRC cells irrespective of their p53 status. Furthermore, we demonstrate that DNA replication stress/DNA damage activates global metabolic alterations in CRC cells that help them to deal with the genome injury. These data are congruent with the finding that DDR signaling can activate SIRT1/AMPK/PGC1 $\alpha$ -mediated molecular pathways to increase mitochondrial functions and biogenesis [50–52]. Similar with our data, others found with the MTT assay that a direct induction of DNA breaks by  $\gamma$ -irradiation augmented ETC CII activity and mitochondrial biogenesis in cervix and breast cancer cells [53]. According to our data, irinotecan increases the ETC activity and causes an accumulation of ETC complexes that requires apparently increased translation of reduced amounts of mitochondrial mRNAs. These data suggest that irinotecan promotes the ETC activity differently from  $\gamma$ -irradiation-induced DNA damages and likely independent of mitochondrial

(See figure on next page.)

**Fig. 4** Glucose restriction sensitizes p53-proficient HCT116 cells to irinotecan. **A** p53 wild-type (HCT<sup>wt</sup>) and isogenic p53 null (HCT<sup>Δp53</sup>) HCT116 cells were exposed to 10  $\mu$ M irinotecan (Iri). The abundance of indicated metabolites was assessed after 24 h by targeted mass spectrometric analysis (metabolomics) (refer to Fig. 3). Changes of individual metabolites are summarized for the HCT116 cell lines. Green/red color indicates a higher/lower abundance after irinotecan treatment, respectively. Black indicates no change after treatment. If not further specified, metabolites in both HCT<sup>wt</sup> (wt) and HCT<sup>Δp53</sup> ( $\Delta$ p53) were altered in the same way. Abbreviations: ETC electron transport chain, PPP pentose phosphate pathway, ROS reactive oxygen species, GSH/GSSG reduced/oxidized glutathione, PEP phosphoenolpyruvate. **C–E** HCT<sup>wt</sup> and isogenic HCT<sup>Δp53</sup> cells cultured in DMEM with high (4.5 g/l) or low (1 g/l) glucose were exposed to 10  $\mu$ M Iri. The loss of mitochondrial membrane potential (loss of  $\Delta\Psi_M$ ) and cell death was analyzed by flow cytometry after 24 h (**B**) and 48 h (**D**). The oxygen consumption of HCT<sup>wt</sup> cells was assessed after 24 h (**C**) and 48 h (**E**) using a Clarke electrode. **B, D** The average of 4 individual experiments  $\pm$  SEM. **C, E** The average of 2 individual experiments  $\pm$  SEM. Statistics for this figure: \* $p < 0.05$ ; \*\* $p < 0.01$

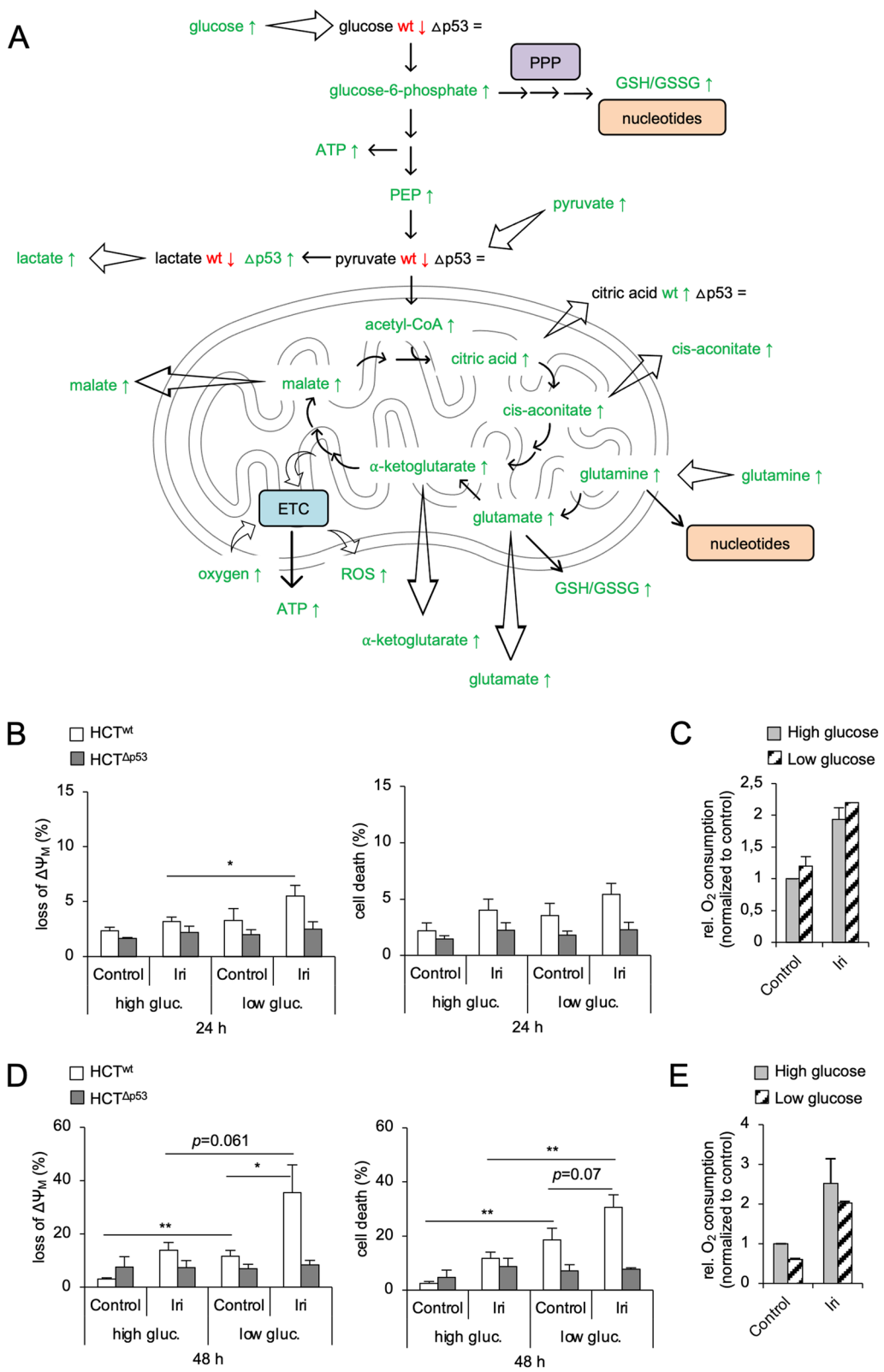


**Fig. 4** (See legend on previous page.)

biogenesis. Further studies are necessary to reveal if direct DNA damage ( $\gamma$ -irradiation) changes mitochondrial functions differently compared to DNA replication stress and indirect DNA damage (irinotecan). Moreover, cell type-specific differences may determine how mitochondria respond to DNA replication stress and DNA damage.

Our Seahorse analysis unraveled that HCT116 cells increased both their glycolysis and respiration during DNA replication stress. HCT116<sup>wt</sup> cells had in general a higher metabolism than p53-deficient cells and preferentially increased their glycolysis during DNA replication stress when glucose was available. This is in line with a recent study in hepatocellular carcinomas (HCCs) [31] but in contrast to the classical view on p53-mediated metabolic changes in response to stress [8, 9, 29, 30]. The difference may originate from the KRAS<sup>G13D</sup> mutation in HCT116 cells. CRC tumors and cell lines have frequently mutations in *KRAS* leading to metabolic reprogramming, including an increased glycolysis, PPP activity, and glutaminolysis, making them reliant on these pathways [10, 41, 54–56]. In comparison, p53 and *KRAS* wild-type RKO cells [57] just increased their respiration due to irinotecan-induced DNA replication stress, without prominent effects on their glycolysis. The metabolic rewiring due to *KRAS* mutations in CRC translates into differential activation of molecular signaling pathways like mTOR and AMPK and causes metabolic maladaptation in patients [10, 41, 54, 55]. This should be considered for personalized treatment approaches that target the tumor metabolism in parallel to classical chemotherapy.

Using a customized Seahorse analysis, we demonstrate that HCT116 cells do not reconstitute their OXPHOS activity after mitochondrial uncoupling via cyanide-4-(trifluoromethoxy)-phenylhydrazine (FCCP) injection when glucose is available. Nevertheless, when cells are glucose-restricted, they use pyruvate to selectively fuel their TCA cycle and OXPHOS. Thus, they have a greater basal OCR than before and show a strong respiratory spare capacity after mitochondrial uncoupling. This indicates that HCT116 cells generate their energy solely from glycolysis when their mitochondrial ATP synthase is inhibited by the injection of oligomycin. In the Mito Stress Test, they do not rescue their mitochondrial membrane potential by increasing their OXPHOS after mitochondrial uncoupling. This highlights the addiction of HCT116 cells to glucose as their key energy source, being a textbook example of a colorectal cancer showing the Warburg effect [1, 5–7]. When glucose is not available, these cells are forced to utilize their mitochondrial potential more extensively.

We further reveal that the irinotecan-induced mitochondrial activity led to high ROS levels. Regarding ROS,

p53 is a well-known regulator of cell metabolism and the antioxidant response [8–10, 29]. Confirming this notion, less ROS accumulated in HCT116<sup>wt</sup> cells after irinotecan treatment compared with their p53-deficient counterparts, although HCT116<sup>wt</sup> showed a stronger OXPHOS increase. This tied in with a more pronounced reduction of *MT-COII*, *MT-ND1*, and *MT-CYB* in irinotecan-treated HCT116 cells lacking p53. ROS originate mainly from ETC CI and CIII during OXPHOS and damage the mtDNA directly [3, 18, 19, 37, 40, 41, 43, 58–61]. Hence, ROS accumulation and damage to mtDNA might explain why irinotecan attenuated the expression of mitochondrial mRNAs.

This work provides evidence that drugs that evoke DNA replication stress and DNA damage promote metabolic adaptations. Intriguingly, we noted that irinotecan enhanced the protein expression of ETC complex subunits in vivo and in vitro. Chloramphenicol, which is an inhibitor of mitochondrial ribosomes [42], reduced the expression of ETC CI-IV and the irinotecan-induced abundance of ETC proteins and respiration in HCT116 cells. Thus, the higher level of ETC complex subunits during irinotecan-induced DNA replication stress likely originated from increased mitochondrial protein translation, and not from increased mtDNA-encoded mRNA levels or an accumulation of mitochondria. However, further studies will be necessary to consolidate this finding. The mitochondrial DNA harbors TOP1mt, which strictly locates to mitochondria, and they import Top2 $\beta$  and Top3 $\alpha$  to solve topological stress [62, 63]. The nuclear topoisomerase TOP1 is not found in mitochondria. Nevertheless, there is evidence that camptothecin (CPT) can inhibit both TOP1 and TOP1mt [64, 65]. This might also apply to the CPT derivate irinotecan (CPT-11) [32, 46, 64] and give an additional explanation for the reduced mtDNA expressions in irinotecan-treated cells.

We validated our biochemical analysis on cell metabolism during DNA replication stress by a targeted metabolomics approach. We found an increased turnover of metabolites from the glycolysis, PPP, and TCA cycle in both HCT116 cell lines. This led to a higher consumption of energy sources from the environmental cell culture medium, increased intracellular metabolite levels, and ATP production. Others have consistently shown that suppression of the cancer cell metabolism, at the levels of mtDNA translation, glucose or glutamine metabolism, can augment the effectiveness of chemotherapy [3, 14, 15, 18, 19, 25–28, 42, 47, 56, 66, 67]. Moreover, in response to mtDNA damage, cancer cells can increase their glutamine metabolism for compensation [19] and metabolic adaptation of the TCA cycle is required for tumor growth in vivo [12]. As expected from these insights, both HCT116 cell lines increase their glutamine metabolism

in response to irinotecan. This metabolic adaptation can feed the TCA and OXPHOS for energy production, and it is in addition to the PPP, another source for nucleotide and glutathione de novo synthesis [2, 14, 19, 30, 54, 56]. Glutathione is an essential endogenous ROS scavenger and nucleotides are necessary for the repair of DNA damage during chemotherapy [15, 30, 56, 68, 69]. Hence, their production through different metabolic pathways might help CRC cells to deal with DNA replication stress, and an abrogated glucose metabolism appears attractive to increase the effectiveness of chemotherapy.

Interestingly, HCT116<sup>wt</sup> cells deplete their intracellular glucose and pyruvate levels during DNA replication stress and glucose is a limiting factor for the survival of irinotecan-treated HCT116<sup>wt</sup> cells. This was also reflected by the OXPHOS activity of HCT116<sup>wt</sup> cells cultured for 48 h in DMEM with low glucose compared with cells in a high-glucose medium. Isogenic p53-deficient cells use their glucose more economically and were significantly less affected by irinotecan under both high- and low-glucose cell culture conditions. Thus, the high metabolism in HCT116<sup>wt</sup> cells might protect them from toxic DNA damage if glucose is available, which makes them in turn vulnerable to an absence of this energy source.

## Conclusions

Global analyses illustrate that the irinotecan-induced DNA replication stress/DNA damage leads to metabolic adaptation of CRC cells, including increased OXPHOS, glycolysis, glutaminolysis, TCA, and PPP activity. Hence, exploiting CRC metabolism can be a promising approach to increase the effectiveness of irinotecan and other DNA replication stress-inducing agents in p53-proficient CRC cells.

## Methods

### Reagents

Irinotecan hydrochloride, 2-thenoyltrifluoroacetone (TTFA), hydroxyurea (HU), 2',7'-dichlorofluorescein diacetate (DCFDA), 3-(4,5-dimethylthiazol-2-yl)-2,5-diphenyltetrazolium bromide (MTT), 2-deoxy-D-glucose (2-DG), crystal violet, and antimycin A were purchased from Sigma Aldrich (Deisenhofen, Germany). Doxorubicin was purchased from Enzo Life Science (Lörrach, Germany). Chloramphenicol was purchased from Carl Roth GmbH (Karlsruhe, Germany). Rotenone, carbonyl cyanide-4-(trifluoromethoxy)phenylhydrazone (FCCP), and oligomycin were purchased from Abcam (Cambridge, UK). 3,3'-Dihexyloxycarbocyanine iodide (DiOC<sub>6</sub>(3)) was purchased from Thermo Fisher Scientific

(Waltham, MA, USA). DMSO was used as a treatment control.

### Cell culture

HCT116 wild-type and otherwise isogenic cell lines lacking p53 cells were a gift from Dr. B. Vogelstein (Baltimore, MD, USA). RKO ATCC cells were received from the DSMZ Braunschweig and a gift of Dr. M. Zörnig (Frankfurt/Main, Germany). Cells were maintained in high-glucose (4.5 g/l) DMEM with stable glutamine, 10% fetal calf serum (FCS), and 100 U/ml penicillin/streptomycin (all from Thermo Scientific). Cells were cultivated at 37 °C in a humidified 5% CO<sub>2</sub> incubator and routinely passaged.

Experiments were performed in high-glucose (4.5 g/l) or low-glucose (1 g/l) DMEM with stable glutamine and 10% fetal calf serum (all from Thermo Scientific) without antibiotics. Cells were treated with 10 μM irinotecan, 1 mM HU, 1 μM doxorubicin, 0.1 mM TTFA, 0.1 μM rotenone, or 0.1 mg/ml chloramphenicol for up to 48 h.

### Flow cytometric analysis of cell death and mitochondrial transmembrane potential ( $\Delta\Psi_M$ )

Analysis was performed as described in [70].

### Flow cytometric analysis of reactive oxygen species (ROS)

Analysis was performed as described in [70].

### MTT cell viability assays

MTT assays were performed as described in [70]. In parallel, cell numbers were counted using a Particle Counter Z1 (Beckman Coulter) and the obtained MTT values were normalized to corresponding cell numbers.

### Analysis of O<sub>2</sub> consumption

Detached cells were counted with a hemocytometer (Paul Marienfeld GmbH & Co. KG, Lauda Königshofen, Germany) centrifuged and resuspended to a final concentration of  $3 \times 10^6$  cells per ml in high-glucose DMEM. One milliliter of this suspension was transferred into a Clarke electrode (Oxygraph system, Hansatech-instruments, Norfolk, UK). O<sub>2</sub> consumption was measured by the decrease of oxygen within the chamber during a 5-min time period.

### Seahorse analysis of cells

#### Cell Mito Stress Test

The supernatant medium was replaced with a Seahorse XF base medium (Agilent Technologies, pH adjusted to 7.4), supplemented with 10 mM D-glucose (Sigma Aldrich), 2 mM L-glutamine, and/or 1 mM sodium pyruvate (both from Thermo Scientific). Cells were then

incubated for additional 1 h in a CO<sub>2</sub>-free incubator at 37 °C. Basal oxygen consumption rate (OCR) and extracellular acidification rate (ECAR) were measured with a Seahorse XFe24 Analyzer (Agilent Technologies) before consecutively adding 2 μM oligomycin, 2 μM FCCP, and 2 μM antimycin A. In this assay, basal OCR and ECAR values are measured before different ETC inhibitors are injected consecutively during the analysis. Oligomycin blocks ETC CV to analyze the amount of OCR used to generate ATP. FCCP chemically disrupts the mitochondrial membrane integrity and membrane potential ( $\Delta\Psi_M$ ) to uncouple the respiration, usually leading to a maximal increase in OCR and ECAR [44, 45]. Antimycin A inhibits ETC CIII (cytochrome *c* reductase) and thus the electron transport from ETC CI/II into CIV. This finally breaks down the mitochondrial respiration [44, 45].

#### **Glycolysis Stress Test**

The supernatant medium was replaced with a Seahorse XF base medium (pH adjusted to 7.4), supplemented with 2 mM L-glutamine. Cells were then incubated for additional 1 h in a CO<sub>2</sub>-free incubator at 37 °C. Basal OCR and ECAR were measured with a Seahorse XFe24 Analyzer before consecutively adding 10 mM D-glucose, 2 μM oligomycin, and 50 mM 2-deoxy-D-glucose (2-DG). In this assay, D-glucose is added to analyze the resulting increase of ECAR. Oligomycin blocks the OXPHOS and in consequence induces high ECAR in cells to maintain their overall energy production. 2-Deoxy-D-glucose (2-DG), which is a competitive inhibitor of hexokinase and glucose-6-phosphate isomerase [48], breaks down the glycolysis and resulting ECAR.

In both assays, OCR and ECAR were measured as pmol/min and mpH/min, respectively, in cycles of 3-min mix and 3-min measure periods at 37 °C. At the end of the measurement, cell densities per well were quantified by crystal violet staining (performed as described in [70]) and the observed OCR and ECAR were normalized to corresponding cell densities. Wave software (Agilent Technologies) was used to analyze the datasets.

#### **Quantitative real-time RT-PCR**

Total RNA was isolated using the Peggold Total RNA Kit including DNase digestion (Peglab, Erlangen, Germany). RNA was transcribed into cDNA using Omniscript (Qiagen, Hilden, Germany). Quantitative PCR for *MT-COII*, *MT-ND1*, and *MT-CYB* was performed using the Applied Biosystems (Darmstadt, Germany) 7900HT Real-Time PCR system. Expression levels were normalized to β2-microglobulin. Reactions were done in duplicate using Applied Biosystems Gene Expression Assays (COX2: Hs02596865\_g1, NDH: Hs02596873\_s1, CYTB:

Hs02596867\_s1, β-2-microglobulin: Hs00187842\_m1) and Universal PCR Master Mix. All procedures were performed according to the manufacturers' protocols. The relative gene expressions were calculated by the 2<sup>(-ΔΔCt)</sup> method.

#### **Tumor resection lysates**

Resection specimens of human CRC xenografts were obtained from mice as described in [38]. Mice were bred in the animal facility of the University Medical Center in Rostock under specific pathogen-free conditions. During their whole lifetime, all animals got enrichment in the form of mouse-igloos (ANT Tierhaltungsbedarf, Buxtehude, Germany), nesting material (shredded tissue paper, Verbandmittel GmbH, Frankenberg, Germany), paper roles (75 × 38 mm, H 0528–151, ssniff-Spezialdiäten GmbH, Cologne, Germany), and wooden sticks (40 × 16 × 10 mm, Abedd, Vienna, Austria). During the experiment, mice were kept in type III cages (Zoonlab GmbH, Castrop-Rauxel, Germany) at 12-h dark:light cycle, the temperature of 21 ± 2 °C, and relative humidity of 60 ± 20% with food (pellets, 10 mm, ssniff-Spezialdiäten GmbH, Soest, Germany) and tap water ad libitum. Tumor resection specimens were homogenized in radioimmunoprecipitation assay (RIPA) buffer (50 mM Tris/HCl (pH 8.0), 150 mM NaCl, 1 mM EDTA, 1% NP-40, 1% sodium deoxycholate, and 0.1% SDS; supplemented with a protease inhibitor cocktail and 0.5 mM PMSF) followed by rigorous sonication. Protein quantification was done by Pierce BCA Protein Assay Kit (Thermo Scientific) following the manufacturer's instruction.

#### **Whole cell lysates**

Cell lysates were prepared as described in [70]. Protein quantification was done by Pierce BCA Protein Assay Kit (Thermo Scientific) following the manufacturer's instruction.

#### **Mitochondrial isolation**

Mitochondria were isolated as described in [71].

#### **Immunoblotting**

Ten to 20 μg of protein per lane was separated by standard SDS-PAGE and transferred onto PVDF membranes. After blocking in blocking solution (BS; 100 mM Tris/HCl (pH 8.0), 450 mM NaCl, 5% dry milk, and 0.05% Tween-20), the membranes were incubated with antibodies against Total OXPHOS Human WB Antibody Cocktail (1:5000 in BS, Abcam), TOM40 (1:5000), p53 (1:5000 in BS, both from Santa Cruz Biotechnology, Dallas, TX, USA), and phospho-Ser139 Histone H2AX (γH2AX) (1:5000 in BS, Millipore/Merck KGaA, Darmstadt,

Germany). Equal loading of whole cell lysates was verified by the detection of HSP90 (1:5000 in BS, Santa Cruz). Peroxidase-conjugated anti-mouse IgG (H+L) and anti-rabbit IgG (H+L) secondary antibodies (1:10,000; Abcam) were used and detection of specific signals was done with SuperSignal West Pico Chemiluminescent Substrate (Pierce/Thermo Scientific). Densitometric quantification was done with ImageJ (National Institutes of Health, Bethesda, MD, USA). Full immunoblot images are depicted in supplementary Fig. S4.

### Mass spectrometric analysis (metabolomics)

LC–MS analysis was performed as described in [30, 49]. Metabolites were extracted from supernatant media before and after treatment and by lysing cells in ice-cold methanol/acetonitrile/H<sub>2</sub>O (50:30:20). Samples were shaken at 4 °C for 10 min and then centrifuged for 15 min at 16,000 g, and the supernatant was collected and analyzed by LC–MS. Analytes were separated using hydrophilic interaction liquid chromatography with a SeQuant ZIC-pHILIC column (2.1 × 150 mm, 5 mm) (Merck) and detected with high-resolution, accurate-mass mass spectrometry using an Orbitrap Exactive in line with an Accela autosampler and an Accela 600 pump (Thermo Scientific). The elution buffers were acetonitrile for buffer A and 20 mM (NH<sub>4</sub>)<sub>2</sub>CO<sub>3</sub> and 0.1% NH<sub>4</sub>OH in H<sub>2</sub>O for buffer B. A linear gradient was programmed starting from 80% buffer A and ending at 20% buffer A after 20 min, followed by wash (20% buffer A) and re-equilibration (80% buffer A) steps with a flow rate of 100 ml/min. The mass spectrometer was fitted with an electrospray-ionization probe and operated in full-scan and polar-switching mode with the positive voltage at 4.5 kV and negative voltage at 3.5 kV. Metabolite identification and data analysis were carried out using LCQUAN software (Thermo Scientific).

### Statistical analysis

Statistical analyses were done using two-tailed Student's *t* test with Microsoft Excel (\**p* < 0.05, \*\**p* < 0.01, \*\*\**p* < 0.001). All values are displayed as mean ± SEM.

### Abbreviations

AMPK: 5' Adenosine monophosphate (AMP)-activated protein kinase; ATP: Adenosine triphosphate; Chlor: Chloramphenicol; COX: Cytochrome *c* oxidase; CPT: Camptothecin; CRC: Colorectal cancer cells; DCFDA: 2',7'-Dichlorofluorescein diacetate; ECAR: Extracellular acidification rate; ETC: Electron transport chain; ETC CI-V: ETC complex I-V; FCCP: Carbonyl cyanide-4-(trifluoromethoxy)-phenylhydrazone; GSH/GSSG: Reduced/oxidized glutathione; γH2AX: Phosphorylated histone protein H2AX; HCC: Hepatocellular carcinoma; HCT116<sup>wt</sup>: HCT116 cell line expressing wild-type p53 (wt); HCT116<sup>Δp53</sup>: HCT116 cell line with p53 deletion (Δp53; p53 null; p53<sup>-/-</sup>); HROC: Hanses-tadt Rostock colon cancer; HU: Hydroxyurea; Iri: Irinotecan (CPT-11); KRAS: Kirsten rat sarcoma virus; MMP (ΔΨ<sub>m</sub>): Mitochondrial membrane potential; mtDNA: Mitochondrial DNA; mTOR: Mechanistic target of rapamycin; MTT:

3-(4,5-Dimethylthiazol-2-yl)-2,5-diphenyltetrazolium bromide; NDH: NADH dehydrogenase; OCR: Oxygen consumption rate; OXPHOS: Oxidative phosphorylation; PEP: Phosphoenolpyruvate; PGC1α: Peroxisome proliferator-activated receptor gamma coactivator 1-α; PPP: Pentose phosphate pathway; qPCR: Quantitative polymerase chain reaction; RNR: Ribonucleotide reductase; ROS: Reactive oxygen species; SDH: Succinate dehydrogenase; SIRT1: Sirtuin 1; TCA: Tricarboxylic acid cycle; TOP1: Topoisomerase-1; TOP1mt: Mitochondrial topoisomerase-1; TOP2: Topoisomerase-2; TTFa: 2-Thenoyltrifluoroacetone.

### Supplementary Information

The online version contains supplementary material available at <https://doi.org/10.1186/s40170-022-00286-9>.

**Additional file 1: Fig. S1.** (A-B) p53 wild-type (HCT<sup>wt</sup>) and isogenic p53 null (HCT<sup>Δp53</sup>) HCT116 cells were exposed to 10 μM irinotecan (Iri). (A) The expression of indicated proteins in whole cell lysates was analyzed after 24 h by Western blot. HSP90 was used to control equal protein loading. (B) The oxygen consumption of cells was assessed at indicated time points after treatment using a Clarke electrode. (C) HROC24 and HROC87 patient-derived short term colorectal cancer cells were xenotransplanted into mice and treated with Iri or control (see methods). The expression of indicated proteins in tissue lysates of tumor resections was analyzed by Western blot. The expression of electron transport chain (ETC) complex subunits relative to complex V was quantified by densitometry using ImageJ and is depicted next to the immunoblots. (D) MTT assays were performed, and corresponding cell numbers counted in parallel to calculate the MTT turnover/cell number (refer to Fig. 1D). HCT<sup>Δp53</sup> (E) and HCT<sup>wt</sup> (F) cells were exposed to 10 μM Iri, 1 μM hydroxyurea (HU), 1 μM doxorubicin (Doxo), 0.1 mM TTFa, 0.1 μM rotenone (Rot) or 0.1 mg/ml chloramphenicol (Chlor) as single agents and in combination for 24 h. The oxygen consumption of cells was assessed using a Clarke electrode. (A) is representative of 2 individual experiments. (C) The number of individual experimental repeats is depicted within the graphs/bars representing their average ± SEM. (B, D-F) show the average of 3 individual experiments ± SEM. Statistics for this figure: \* *p* < 0.05; \*\* *p* < 0.01; \*\*\* *p* < 0.001.

**Additional file 2: Fig. S2.** (A-B) p53 wild-type (HCT<sup>wt</sup>) and isogenic p53 null (HCT<sup>Δp53</sup>) HCT116 cells were exposed to 10 μM irinotecan (Iri) for 24 h. Oxygen consumption (OCR) and extracellular acidification rates (ECAR) were assessed using a Seahorse XFe24 Analyzer. The workflow of a standard Cell Mito Stress Test is depicted in (A). (B) Basal OCR and ECAR values were calculated from curves shown in Fig. 2A-B. (C-E) p53 wild-type RKO cells were exposed to 10 μM irinotecan (Iri) for 24 h. (C) Oxygen consumption (OCR) and (D) extracellular acidification rates (ECAR) were assessed with a Cell Mito Stress Test using a Seahorse XFe24 Analyzer. 2 μM oligomycin, 2 μM FCCP and 2 μM antimycin A were injected consecutively during the measurement. (E) Bioenergetic parameters, i.e., ATP production and respiratory spare capacity, were calculated from OCR/ECAR curves shown in (C-D). (F-G) HCT<sup>wt</sup> and HCT<sup>Δp53</sup> cells were exposed to 10 μM irinotecan (Iri) for 24 h. Oxygen consumption (OCR) and extracellular acidification rates (ECAR) were assessed using a Seahorse XFe24 Analyzer. The workflow of a Glycolysis Stress Test is depicted in (F). (G) The glutamine- and glucose-driven OCR calculated from curves shown in Fig. 2D. Abbreviations: mitochondrial membrane potential (MMP), electron transport chain (ETC), glutamine (gln), glucose (glu) and pyruvate (pyr). (B, G) show the average of 3 individual experiments ± SEM. (C-E) show the average of 2 individual experiments ± SEM. Statistics for this figure: \* *p* < 0.05; \*\* *p* < 0.01; \*\*\* *p* < 0.001.

**Additional file 3: Fig. S3.** p53 wild-type (HCT<sup>wt</sup>) and isogenic p53 null (HCT<sup>Δp53</sup>) HCT116 cells were exposed to 10 μM irinotecan (Iri) for 24 h. The workflow of a custom Cell Mito Stress Test in the absence of pyruvate is depicted in (A). (B) Oxygen consumption (OCR) and (C) extracellular acidification rates (ECAR) were assessed using a Seahorse XFe24 Analyzer. 2 μM oligomycin, 2 μM FCCP and 2 μM antimycin A were injected consecutively during the measurement. (D) Basal OCR and ECAR values were calculated from curves shown in (B-C). (E) Bioenergetic parameters, i.e., ATP production and respiratory spare capacity, were calculated from OCR/ECAR curves shown in (B-C). The workflow of a custom Cell Mito

Stress Test in the absence of glucose is depicted in (F). (G) OCR and (H) ECAR were assessed using a Seahorse XFe24 Analyzer. 2  $\mu$ M oligomycin, 2  $\mu$ M FCCP and 2  $\mu$ M antimycin A were injected consecutively during the measurement. (I) Basal OCR and ECAR values were calculated from curves shown in (G-H). (J) Bioenergetic parameters, i.e., ATP production and respiratory spare capacity, were calculated from OCR/ECAR curves shown in (G-H). Abbreviations used: mitochondrial membrane potential (MMP), electron transport chain (ETC), glutamine (gln), glucose (glu) and pyruvate (pyr). The data presented in (B-E) and (G-J) were generated side-by-side, and all values are normalized to control values of HCT<sup>wt</sup> cells in (B) and (C), respectively. All graphs show the average of 3 individual experiments  $\pm$  SEM. Statistics for this figure: \*  $p < 0.05$ ; \*\*  $p < 0.01$ ; \*\*\*  $p < 0.001$  within each panel; <sup>o</sup>  $p < 0.05$ ; <sup>oo</sup>  $p < 0.01$ ; <sup>ooo</sup>  $p < 0.001$  in comparison between (D) and (I) as well as (E) and (J), respectively.

**Additional file 4: Fig. S4.** (A) and (B) show the full immunoblots used to assemble figures 1B and 1H, respectively. (C) and (D) show the full immunoblots used to assemble supplementary figures S1B and S1C, respectively. Black boxes indicate the cropped portion of each immunoblot shown in the corresponding main figures. Immunoblots shown in (D) were detected using a LI-COR Odyssey<sup>®</sup> detection system. All other figures were detected using ECL and X-ray films.

### Acknowledgements

We like to thank Dr. Karen Vousden explicitly for offering C.M. the opportunity to work in her lab and Gillian M. Mackay for performing mass spectrometry analysis. We like to thank Sigrid Reichard and Sabine Scheiding for technical support. This work includes parts of the PhD thesis of C.M.

### Authors' contributions

C.M. performed most experiments. J.S. and L.M.-B. performed qPCR and Clarke electrode measurements; O.D.K.M. performed targeted mass spectrometry analysis; M.B. performed several immunoblots; D.H. performed Clarke electrode measurements; C.I.M. performed animal experiments; O.D.K.M., J.S., R.T., M.L., and T.H. contributed to the scientific development, discussion, and supervision of the project. C.M. and O.H.K. designed the experiments, interpreted the data, supervised the project, and wrote the manuscript. The authors read and approved the final manuscript.

### Funding

Open Access funding enabled and organized by Projekt DEAL. This project was funded by DFG project RTG1715 SP13 (to O.H.K.). C.M. had additional funding from Boehringer Ingelheim Fonds (BIF) and Richard Winter Stiftung (both to C.M.). ODKM was funded by CRUK Career Development Fellowship C53309/A19702. L.M.-B. was supported by a scholarship of the Graduate Academy (GA) of the Friedrich Schiller University (FSU) Jena. Work done in the lab of O.H.K. is supported by the Deutsche Forschungsgemeinschaft KR2291/9-1, project number 427404172/12-1, project number 445785155/14-1, project number 469954457/15-1, project number 495271833, project number 496927074/16-1, DFG-project number 393547839—SFB 1361, sub-project 11, the Wilhelm Sander-Stiftung (2019.086.1), and the Brigitte und Dr. Konstanze Wegener-Stiftung (Projekt #65).

### Availability of data and materials

Metabolomics datasets used and analyzed during the current study are available from the corresponding author on reasonable request. Otherwise, all data generated or analyzed during this study are included in this published article (and its supporting information files).

### Declarations

#### Ethics approval and consent to participation

All animal experiments were approved by the German local authority: "Landesamt für Landwirtschaft, Lebensmittelsicherheit und Fischerei Mecklenburg-Vorpommern" (approval number: LALLF M-V/VTSD/7221.3-1.1-071-10), under the German animal protection law and the EU Guideline 2010/63/EU.

#### Consent to publication

Not applicable.

### Competing interests

Oliver Maddocks declares to be a co-founder, board member, and shareholder of Faeth Therapeutics.

### Author details

<sup>1</sup>Department of Toxicology, University Medical Center, Johannes Gutenberg University Mainz, Building 905, Mainz, Germany. <sup>2</sup>Department of Biochemistry, Center for Molecular Biomedicine (CMB), Institute for Biochemistry and Biophysics, Friedrich Schiller University of Jena, Jena, Germany. <sup>3</sup>Leibniz Institute on Aging - Fritz Lipmann Institute (FLI), Jena, Germany. <sup>4</sup>Current Address: Center for Pandemic Vaccines and Therapeutics (ZEPAT), Paul Ehrlich Institute, Langen, Germany. <sup>5</sup>Department of Paediatric Haematology and Oncology, Jena University Hospital, Children's Clinic, Jena, Germany. <sup>6</sup>Research Center Lobeda, Jena University Hospital, Jena, Germany. <sup>7</sup>Wolfson Wohl Cancer Research Centre, Institute of Cancer Sciences, University of Glasgow, Glasgow, UK. <sup>8</sup>Department of Human Nutrition, Institute of Nutrition, Friedrich Schiller University of Jena, Jena, Germany. <sup>9</sup>Current address: Biopharmaceutical New Technologies (BioNTech) Corporation, Mainz, Germany. <sup>10</sup>Molecular Oncology and Immunotherapy, Thoracic, Vascular and Transplantation Surgery, Clinic of General, University of Rostock, VisceralRostock, Germany. <sup>11</sup>Current address: Department of Medicine, Clinic III - Hematology, Oncology, Palliative Medicine, Rostock University Medical Center, Rostock, Germany.

Received: 11 January 2022 Accepted: 9 June 2022

Published online: 04 July 2022

### References

- Cassim S, Vucetic M, Zdravlevic M, Pouyssegur J. Warburg and beyond: the power of mitochondrial metabolism to collaborate or replace fermentative glycolysis in cancer. *Cancers (Basel)* 2020;12(5):1119.
- Ge T, Yang J, Zhou S, Wang Y, Li Y, Tong X. The role of the pentose phosphate pathway in diabetes and cancer. *Front Endocrinol (Lausanne)* 2020;11:365.
- Guerra F, Arbini AA, Moro L. Mitochondria and cancer chemoresistance. *Biochim Biophys Acta Bioenerg* 2017;1858(8):686–99.
- Huttemann M, Lee I, Grossman LI, Doan JW, Sanderson TH. Phosphorylation of mammalian cytochrome c and cytochrome c oxidase in the regulation of cell destiny: respiration, apoptosis, and human disease. *Adv Exp Med Biol* 2012;748:237–64.
- Diaz-Ruiz R, Rigoulet M, Devin A. The Warburg and Crabtree effects: on the origin of cancer cell energy metabolism and of yeast glucose repression. *Biochim Biophys Acta* 2011;1807(6):568–76.
- Lu J, Tan M, Cai Q. The Warburg effect in tumor progression: mitochondrial oxidative metabolism as an anti-metastasis mechanism. *Cancer Lett* 2015;356(2 Pt A):156–64.
- Koppenol WH, Bounds PL, Dang CV. Otto Warburg's contributions to current concepts of cancer metabolism. *Nat Rev Cancer* 2011;11(5):325–37.
- Gottlieb E, Vousden KH. p53 regulation of metabolic pathways. *Cold Spring Harb Perspect Biol* 2010;2(4):a001040.
- Maddocks OD, Vousden KH. Metabolic regulation by p53. *J Mol Med (Berl)* 2011;89(3):237–45.
- Neitzel C, Demuth P, Wittmann S, Fahrer J. Targeting altered energy metabolism in colorectal cancer: oncogenic reprogramming, the central role of the TCA cycle and therapeutic opportunities. *Cancers (Basel)* 2020;12(7):1731.
- Hanahan D, Weinberg RA. Hallmarks of cancer: the next generation. *Cell* 2011;144(5):646–74.
- Echeverri Ruiz NP, Mohan V, Wu J, Scott S, Kremer M, Benej M, Golias T, Papandreou I, Denko NC. Dynamic regulation of mitochondrial pyruvate metabolism is necessary for orthotopic pancreatic tumor growth. *Cancer Metab* 2021;9(1):39.
- Desbats MA, Giacomini I, Prayer-Galetti T, Montopoli M. Metabolic plasticity in chemotherapy resistance. *Front Oncol* 2020;10:281.
- Fu S, Li Z, Xiao L, Hu W, Zhang L, Xie B, Zhou Q, He J, Qiu Y, Wen M, et al. Glutamine synthetase promotes radiation resistance via facilitating nucleotide metabolism and subsequent DNA damage repair. *Cell Rep* 2019;28(5):1136–1143 e1134.
- van Gastel N, Spinelli JB, Sharda A, Schajnovitz A, Baryawno N, Rhee C, Oki T, Grace E, Soled HJ, Milosevic J, et al. Induction of a timed

- metabolic collapse to overcome cancer chemoresistance. *Cell Metab* 2020;32(3):391–403.e6.
16. Meyer FB, Marx C, Spangell SB, Thierbach R. Butyrate and metformin affect energy metabolism independently of the metabolic phenotype in the tumor therapy model. *Biomolecules*. 2021;11(12):1831.
  17. Ahn CS, Metallo CM. Mitochondria as biosynthetic factories for cancer proliferation. *Cancer Metab*. 2015;3(1):1.
  18. Fogg VC, Lanning NJ, Mackeigan JP. Mitochondria in cancer: at the crossroads of life and death. *Chin J Cancer*. 2011;30(8):526–39.
  19. Chen Q, Kirk K, Shurubor YI, Zhao D, Arreguin AJ, Shahi I, Valsecchi F, Primiano G, Calder EL, Carelli V, et al. Rewiring of glutamine metabolism is a bioenergetic adaptation of human cells with mitochondrial DNA mutations. *Cell Metab*. 2018;27(5):1007–1025 e1005.
  20. Varghese E, Samuel SM, Liskova A, Samec M, Kubatka P, Busseberg D. Targeting glucose metabolism to overcome resistance to anticancer chemotherapy in breast cancer. *Cancers (Basel)*. 2020;12(8):2252.
  21. Shin YK, Yoo BC, Hong YS, Chang HJ, Jung KH, Jeong SY, Park JG. Upregulation of glycolytic enzymes in proteins secreted from human colon cancer cells with 5-fluorouracil resistance. *Electrophoresis*. 2009;30(12):2182–92.
  22. Schroll MM, LaBonia GJ, Ludwig KR, Hummon AB. Glucose restriction combined with autophagy inhibition and chemotherapy in HCT 116 spheroids decreases cell clonogenicity and viability regulated by tumor suppressor genes. *J Proteome Res*. 2017;16(8):3009–18.
  23. Tarrago-Celada J, Cascante M. Targeting the metabolic adaptation of metastatic cancer. *Cancers (Basel)*. 2021;13(7):1641.
  24. Siegel RL, Miller KD, Goding Sauer A, Fedewa SA, Butterly LF, Anderson JC, Cercek A, Smith RA, Jemal A. Colorectal cancer statistics, 2020. *CA Cancer J Clin*. 2020;70(3):145–64.
  25. Brandhorst S, Longo VD. Fasting and caloric restriction in cancer prevention and treatment. *Recent Results Cancer Res*. 2016;207:241–66.
  26. O'Flanagan CH, Smith LA, McDonnell SB, Hursting SD. When less may be more: calorie restriction and response to cancer therapy. *BMC Med*. 2017;15(1):106.
  27. Nencioni A, Caffa I, Cortellino S, Longo VD. Fasting and cancer: molecular mechanisms and clinical application. *Nat Rev Cancer*. 2018;18(11):707–19.
  28. Deligiorgi MV, Liapi C, Trafalis DT. How far are we from prescribing fasting as anticancer medicine? *Int J Mol Sci*. 2020;21(23):9175.
  29. Liang Y, Liu J, Feng Z. The regulation of cellular metabolism by tumor suppressor p53. *Cell Biosci*. 2013;3(1):9.
  30. Maddocks OD, Berkers CR, Mason SM, Zheng L, Blyth K, Gottlieb E, Vousden KH. Serine starvation induces stress and p53-dependent metabolic remodeling in cancer cells. *Nature*. 2013;493(7433):542–6.
  31. Kim J, Yu L, Chen W, Xu Y, Wu M, Todorova D, Tang Q, Feng B, Jiang L, He J et al. Wild-type p53 promotes cancer metabolic switch by inducing PUMA-dependent suppression of oxidative phosphorylation. *Cancer Cell*. 2019;35(2):191–203 e198.
  32. Thomas A, Pommier Y. Targeting topoisomerase I in the era of precision medicine. *Clin Cancer Res*. 2019;25(22):6581–9.
  33. Vesela E, Chroma K, Turi Z, Mistrik M. Common chemical inductors of replication stress: focus on cell-based studies. *Biomolecules*. 2017;7(1):19.
  34. Yang F, Teves SS, Kemp CJ, Henikoff S. Doxorubicin, DNA torsion, and chromatin dynamics. *Biochim Biophys Acta*. 2014;1845(1):84–9.
  35. Fujita K, Kubota Y, Ishida H, Sasaki Y. Irinotecan, a key chemotherapeutic drug for metastatic colorectal cancer. *World J Gastroenterol*. 2015;21(43):12234–48.
  36. Signes A, Fernandez-Vizcarra E. Assembly of mammalian oxidative phosphorylation complexes I–V and supercomplexes. *Essays Biochem*. 2018;62(3):255–70.
  37. Chaban Y, Boekema EJ, Dudkina NV. Structures of mitochondrial oxidative phosphorylation supercomplexes and mechanisms for their stabilisation. *Biochim Biophys Acta*. 2014;1837(4):418–26.
  38. Maletzki C, Stier S, Gruenert U, Gock M, Ostwald C, Prall F, Linnebacher M. Establishment, characterization and chemosensitivity of three mismatch repair deficient cell lines from sporadic and inherited colorectal carcinomas. *PLoS ONE*. 2012;7(12): e52485.
  39. Prabst K, Engelhardt H, Ringgele S, Hubner H. Basic colorimetric proliferation assays: MTT, WST, and resazurin. *Methods Mol Biol*. 2017;1601:1–17.
  40. Huang Z, Chen Y, Zhang Y. Mitochondrial reactive oxygen species cause major oxidative mitochondrial DNA damages and repair pathways. *J Biosci*. 2020;45:84.
  41. Kudryavtseva AV, Krasnov GS, Dmitriev AA, Alekseev BY, Kardymon OL, Sadritdinova AF, Fedorova MS, Pokrovsky AV, Melnikova NV, Kaprin AD, et al. Mitochondrial dysfunction and oxidative stress in aging and cancer. *Oncotarget*. 2016;7(29):44879–905.
  42. Skrtic M, Sriskanthadevan S, Jhas B, Gebbia M, Wang X, Wang Z, Hurren R, Jitkova Y, Gronda M, Maclean N, et al. Inhibition of mitochondrial translation as a therapeutic strategy for human acute myeloid leukemia. *Cancer Cell*. 2011;20(5):674–88.
  43. Chen Y, McMillan-Ward E, Kong J, Israels SJ, Gibson SB. Mitochondrial electron-transport-chain inhibitors of complexes I and II induce autophagic cell death mediated by reactive oxygen species. *J Cell Sci*. 2007;120(Pt 23):4155–66.
  44. Little AC, Kovalenko I, Goo LE, Hong HS, Kerk SA, Yates JA, Purohit V, Lombard DB, Merajver SD, Lyssiotis CA. High-content fluorescence imaging with the metabolic flux assay reveals insights into mitochondrial properties and functions. *Commun Biol*. 2020;3(1):271.
  45. Lajqi T, Marx C, Hudalla H, Haas F, Grosse S, Wang ZQ, Heller R, Bauer M, Wetzker R, Bauer R. The role of the pathogen dose and PI3Kgamma in immunometabolic reprogramming of microglia for innate immune memory. *Int J Mol Sci*. 2021;22(5):2578.
  46. Bailly C. Irinotecan: 25 years of cancer treatment. *Pharmacol Res*. 2019;148: 104398.
  47. Huisman SA, de Bruijn P, Ghobadi Moghaddam-Helmantel IM, JN IJ, Wiemer EA, Mathijssen RH, de Bruin RW. Fasting protects against the side effects of irinotecan treatment but does not affect anti-tumour activity in mice. *Br J Pharmacol*. 2016;173(5):804–14.
  48. Pajak B, Siwiak E, Soltyka M, Priebe A, Zielinski R, Fokt I, Ziemniak M, Jaskiewicz A, Borowski R, Domoradzki T, et al. 2-Deoxy-d-glucose and its analogs: from diagnostic to therapeutic agents. *Int J Mol Sci*. 2019;21(1):234.
  49. Labuschagne CF, van den Broek NJ, Mackay GM, Vousden KH, Maddocks OD. Serine, but not glycine, supports one-carbon metabolism and proliferation of cancer cells. *Cell Rep*. 2014;7(4):1248–58.
  50. Fang EF, Kassahun H, Croteau DL, Scheibye-Knudsen M, Marosi K, Lu H, Shamanna RA, Kalyanasundaram S, Bollineni RC, Wilson MA, et al. NAD(+) replenishment improves lifespan and healthspan in ataxia telangiectasia models via mitophagy and DNA repair. *Cell Metab*. 2016;24(4):566–81.
  51. Fang EF, Scheibye-Knudsen M, Chua KF, Mattson MP, Croteau DL, Bohr VA. Nuclear DNA damage signalling to mitochondria in ageing. *Nat Rev Mol Cell Biol*. 2016;17(5):308–21.
  52. Turgeon MO, Perry NJS, Poulogiannis G. DNA damage, repair, and cancer metabolism. *Front Oncol*. 2018;8:15.
  53. Rai Y, Pathak R, Kumari N, Sah DK, Pandey S, Kalra N, Soni R, Dwarkanath BS, Bhatt AN. Mitochondrial biogenesis and metabolic hyperactivation limits the application of MTT assay in the estimation of radiation induced growth inhibition. *Sci Rep*. 2018;8(1):1531.
  54. Hutton JE, Wang X, Zimmerman LJ, Slebos RJ, Trenary IA, Young JD, Li M, Liebler DC. Oncogenic KRAS and BRAF drive metabolic reprogramming in colorectal cancer. *Mol Cell Proteomics*. 2016;15(9):2924–38.
  55. Tabuso M, Christian M, Kimani PK, Gopalakrishnan K, Arasaradnam RP. KRAS status is associated with metabolic parameters in metastatic colorectal cancer according to primary tumour location. *Pathol Oncol Res*. 2020;26(4):2537–48.
  56. Altman BJ, Stine ZE, Dang CV. From Krebs to clinic: glutamine metabolism to cancer therapy. *Nat Rev Cancer*. 2016;16(10):619–34.
  57. Yun J, Rago C, Cheong I, Pagliarini R, Angenendt P, Rajagopalan H, Schmidt K, Willson JK, Markowitz S, Zhou S, et al. Glucose deprivation contributes to the development of KRAS pathway mutations in tumor cells. *Science*. 2009;325(5947):1555–9.
  58. D'Souza AD, Parish IA, Krause DS, Kaech SM, Shadel GS. Reducing mitochondrial ROS improves disease-related pathology in a mouse model of ataxia-telangiectasia. *Mol Ther*. 2013;21(1):42–8.
  59. Giachin G, Bouverot R, Acajjaoui S, Pantalone S, Soler-Lopez M. Dynamics of human mitochondrial complex I assembly: implications for neurodegenerative diseases. *Front Mol Biosci*. 2016;3:43.
  60. Gorrini C, Harris IS, Mak TW. Modulation of oxidative stress as an anticancer strategy. *Nat Rev Drug Discov*. 2013;12(12):931–47.
  61. Vogt S, Rhiel A, Weber P, Ramzan R. Revisiting Kadenbach: electron flux rate through cytochrome c-oxidase determines the ATP-inhibitory effect and subsequent production of ROS. *BioEssays*. 2016;38(6):556–67.

62. Das BB, Ghosh A, Bhattacharjee S, Bhattacharyya A. Trapped topoisomerase-DNA covalent complexes in the mitochondria and their role in human diseases. *Mitochondrion*. 2021;60:234–44.
63. Goffart S, Hangas A, Pohjoismaki JLO. Twist and turn-topoisomerase functions in mitochondrial DNA maintenance. *Int J Mol Sci*. 2019;20(8):2041.
64. Pommier Y, Leo E, Zhang H, Marchand C. DNA topoisomerases and their poisoning by anticancer and antibacterial drugs. *Chem Biol*. 2010;17(5):421–33.
65. Zhang H, Pommier Y. Mitochondrial topoisomerase I sites in the regulatory D-loop region of mitochondrial DNA. *Biochemistry*. 2008;47(43):11196–203.
66. Ashton TM, McKenna WG, Kunz-Schughart LA, Higgins GS. Oxidative phosphorylation as an emerging target in cancer therapy. *Clin Cancer Res*. 2018;24(11):2482–90.
67. Frattaruolo L, Brindisi M, Curcio R, Marra F, Dolce V, Cappello AR. Targeting the mitochondrial metabolic network: a promising strategy in cancer treatment. *Int J Mol Sci*. 2020;21(17):6014.
68. Bansal A, Simon MC. Glutathione metabolism in cancer progression and treatment resistance. *J Cell Biol*. 2018;217(7):2291–8.
69. Kennedy L, Sandhu JK, Harper ME, Cuperlovic-Culf M. Role of glutathione in cancer: from mechanisms to therapies. *Biomolecules*. 2020;10(10):1429.
70. Marx-Blumel L, Marx C, Kuhne M, Sonnemann J. Assessment of HDACi-induced cytotoxicity. *Methods Mol Biol*. 2017;1510:23–45.
71. Marx C, Sonnemann J, Beyer M, Maddocks ODK, Lilla S, Hauzenberger I, Piee-Staffa A, Siniuk K, Nunna S, Marx-Blumel L, et al. Mechanistic insights into p53-regulated cytotoxicity of combined entinostat and irinotecan against colorectal cancer cells. *Mol Oncol*. 2021;15(12):3404–29.

## Publisher's Note

Springer Nature remains neutral with regard to jurisdictional claims in published maps and institutional affiliations.

Ready to submit your research? Choose BMC and benefit from:

- fast, convenient online submission
- thorough peer review by experienced researchers in your field
- rapid publication on acceptance
- support for research data, including large and complex data types
- gold Open Access which fosters wider collaboration and increased citations
- maximum visibility for your research: over 100M website views per year

At BMC, research is always in progress.

Learn more [biomedcentral.com/submissions](https://biomedcentral.com/submissions)

